Improving, Modelling and Simulation of Droop Controller for Grid-forming Inverters in DIgSILENT PowerFactory

Phuoc Nguyen Pham
Fraunhofer Institute for Solar Energy Systems ISE
Inverters in Power Systems
Heidenhofstr. 2, 79110 Freiburg, Germany
phuoc.nguyen.pham@ise.fraunhofer.de

Dr. Ammar Salman
Fraunhofer Institute for Solar Energy Systems ISE
Inverters in Power Systems
Heidenhofstr. 2, 79110 Freiburg, Germany
ammar.salman@ise.fraunhofer.de

Roland Singer
Fraunhofer Institute for Solar Energy Systems ISE
Inverters in Power Systems
Heidenhofstr. 2, 79110 Freiburg, Germany
roland.singer@ise.fraunhofer.de

***Abstract*—Since more and more large conventional power plants, based on direct coupled synchronous generators (SGs), will be phased out in the future, frequency stability must be guaranteed. Consequently, grid-forming inverters are needed to ensure the system stability of the future grids. In the joint research project "VerbundnetzStabil", conducted by Fraunhofer ISE and its partners, the stability of a grid system with a high penetration of inverter-based renewable energy sources (RES) is investigated. This paper aims to develop a droop control concept of grid-forming inverters that can stabilize the system under all future grid scenarios (e.g. grid systems can be split into sub-grids with up to 100% RES and high-power transmission). The droop control structure is presented in both synchronous and stationary frames. Moreover, the droop control scheme is modelled and simulated in DIgSILENT PowerFactory with different test cases.**

Keywords— droop control, grid-forming inverters, pulse width modulation (PWM), DIgSILENT PowerFactory.

I. INTRODUCTION

Nowadays, microgrids (MGs) are increasing rapidly, aiming to replace the conventional centralized electricity generation's system in the future. An MG basically involves distributed generations (DGs) and loads that can operate autonomously in islanded mode or collaboratively work with the main grid in grid-connected mode (Fig. 1). Energy resources in MG are mainly RES, e.g. wind power plants, PV farms, as well as fuel cells and battery storage. They are connected to the grid mostly through inverters.

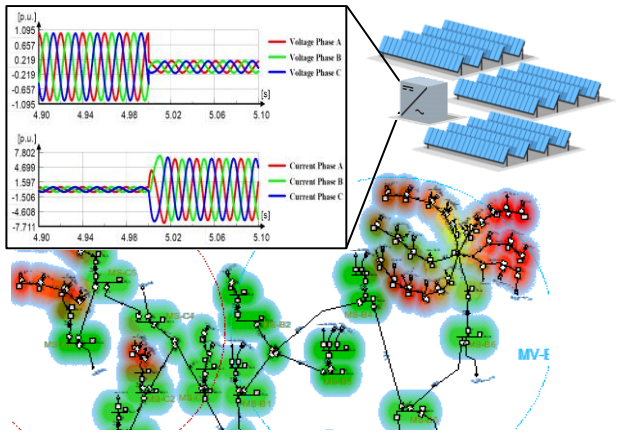

Fig. 1. Grid system model with a high penetration of inverter-based renewable energy sources in DIgSILENT PowerFactory

As a result of the increasing MGs level, the future grid's characteristics, including voltage and frequency will be predominately controlled by the inverters, which are generally classified into two basic types: grid-feeding inverter, as a current source, and grid-forming inverter, as a voltage source. The objective of grid-forming control for voltage source inverters is to ensure the stability of the voltage and frequency of the grid. However, due to the lack of physical inertia, those inverters cannot stabilize the grid during disturbances. To address this issue, grid-forming inverters are integrated with droop control to mimic synchronous generators' behavior in a conventional large-scale network [1]. In this circumstance, the grid-forming inverters will have abilities to regulate voltage and frequency according to active power and reactive power demands. Also, the output current of the inverters should be limited in order to prevent damage to all of the components in case of grid faults.

In this paper, droop control theory for grid-forming inverters is analyzed and simulated by means of DIgSILENT PowerFactory 2020, a software used for power system analysis. This peper is structured as follows:

- Section II is an overview of the droop control theory with an overview control structure.
- Section III is a deep investigation of the voltage and current controls.
- Section IV presents possible current limitation methods.
- Section IV describes a procedure for selecting LCL filter parameters.
- Section VI shows the simulation results of a modelled system in DIgSILENT PowerFactory 2020.
- Finally, section VII concludes the result of this research.

II. OVERVIEW ON DROOP CONTROL STRATEGY

Droop control is a technique for controlling power-sharing in microgrids comprising of inverter-interfaced RES. Unlike the centralized, master–slave, average load sharing or circular chain controls that require high-bandwidth communication channels, droop control implements only using local power measurements, resulting in avoiding high investment cost and improving the MG performance [2], [3]. Moreover, droop control is convenient for the plug-and-play

operation of MGs in which replacing an individual inverter does not affect the whole system. The purpose of using droop control is regulate the frequency and voltage, in which the frequency and output voltage magnitude decrease as the active power and reactive power increase, respectively.

A. Active and reactive power sharing

Referring to Fig. 2, the active power (P) and reactive power (Q) flowing from the inverter to the grid can be written as:

$$P = \frac{EV_g}{X} sin\delta \quad (1)$$

$$Q = \frac{E^2 - EV_g cos\delta}{X} \quad (2)$$

where, E and V_g are the voltage amplitude of the inverter and the grid, respectively, X is the reactance value of line impedance. Considering that the phase angle difference δ is very small, thus, $sin\delta \approx \delta$ and $cos\delta \approx 1$. Therefore, (1) and (2) can be rewritten as:

$$\delta \approx \frac{X}{EV_g} P \quad (3)$$

$$E - V_g \approx \frac{X}{E} Q \quad (4)$$

As shown in (3) and (4), the delivered active power relates to the angle δ and the reactive power is proportional to the voltage difference $(E - V_g)$. However, these relationships are valid only if the interconnection line of the microgrid system is predominantly inductive (i.e. the line resistance R is negligible). In such inductive microgrids, an approximately full decoupling of active power and reactive power can be achieved, which leads to standard droop characteristics that can be described as the equations below:

$$\omega = \omega^* + k_P(P^* - p_m) \quad (5)$$

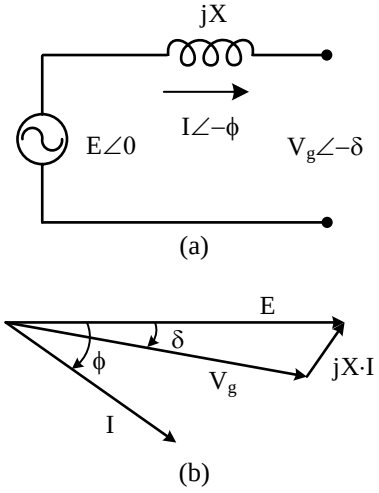

Fig. 2. Modelling of connection between an inverter and the grid. (a) Equivalent circuit. (b) Phasor diagram

$$E = E^* + k_Q(Q^* - q_m) \quad (6)$$

where, ω^* and P^* are the frequency and active power setpoints, respectively, ω is the output frequency, p_m is the measured active power and k_P is the droop slope. Similarly, the inverter output voltage magnitude E is determined by the voltage E^* and reactive power Q^* setpoints, the reactive power measurement q_m and the droop slope k_Q. To participate in frequency and voltage regulation, each grid-forming inverter in the microgrid needs to adjust its power reference according to its droop characteristics [3].

As for low voltage MGs, the feeder impedances might have significantly resistive elements, therefore a change of voltage magnitude or phase will affect both active and reactive power. In this instance, the droop characteristics expressed by (5) and (6) are not valid. The grid-forming inverter implements a so-called virtual output impedance that helps avoid P-Q coupling to the control scheme [4]. Another possible solution is using a P-E/Q-ω droop regulation proposed in [3], [5], which can be added into highly resistive MGs' inverter controllers, however, that case will not be addressed deeply in this paper.

B. Droop control with inertial response

The inertial response is a property of conventional SGs, contributing to the grid's stability. Using stored kinetic energy in rotors, SGs can smooth frequency variations during transient periods to stabilize the system. In contrast, inverters have no natural inertia effect and may cause the system's unstable operation because of the lack of rotating physical mass. To prevent the system from being unstable, virtual inertia is provided to inverters by utilizing a low-pass filter (LPF) filtering the output active power.

$$p_m = \frac{\omega_c}{\omega_c + s} p_o \quad (7)$$

where, ω_c is cut-off frequency, p_o is the output active power and p_m is the measured active power. The cut-off frequency ω_c along with the droop slope k_P establish time and damping constant, which define inertial properties of the inverter [6]. A similar LPF is also applied to reactive power to obtain a smoother voltage reference. Fig. 3 shows a block diagram representing droop control with LPFs.

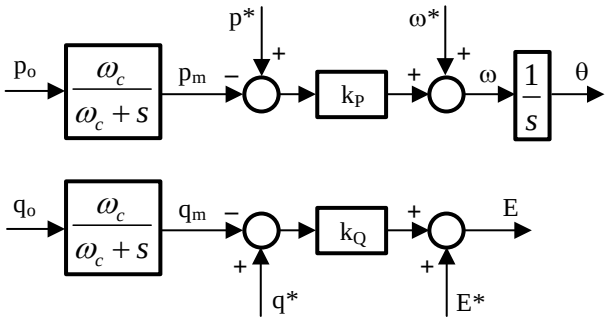

Fig. 3. Block diagram of droop control with LPFs

An overview of the conventional droop controller is demonstrated in Fig. 4. The grid structure consists of an ideal

DC voltage source interfaced through an inverter via an LCL filter. The control scheme includes an outer droop control loop which provides the reference voltage magnitude and frequency. These reference signals pass through an inner control loop comprising cascaded voltage and current control modes. Finally, the output reference voltage of the inner control loop will be utilized to generate pulse-width modulation (PWM) index used to drive the inverter.

III. INVESTIGATION OF CURRENT AND VOLTAGE CONTROL STRATEGIES

Inner current and voltage control loops aim to ensure the zero-error tracking of the output current and voltage reference. The inverter will achieve good performance if the inner current and voltage control loops have fast transient responses and disturbance rejection capability [7]. In this section, two possible controllers are introduced for the inner control loops.

A. Proportional integral (PI) controller on synchronous frame

In a conventional droop controller, the current and voltage control modes are implemented in a synchronous reference frame (dq-frame), in which AC quantities are transformed to DC by using Park transformation. A typical PI controller can be demonstrated as the following equation:

$$G_{PI}(s) = k_p + \frac{k_i}{s} \tag{8}$$

where k_p and k_i are the proportional gain and integral gain, respectively. Due to infinite gain for DC signal, the PI controller proves its ability to track DC reference to achieve zero-error steady-state. However, it also produces some drawbacks:

1) PI controllers require a complex control structure because of the participation of Park and inverse Park transformations, resulting in complicated implementation.

2) The transformation of AC signals to DC signals utilizing Park transformation works incorrectly during transient disturbances, causing the system's instability. This is explained by considering the output of the Park transformation as in (9).

$$\begin{bmatrix} x_d \\ x_q \end{bmatrix} = |x| \begin{bmatrix} cos(\theta_0 - \theta_p) \\ sin(\theta_0 - \theta_p) \end{bmatrix} \tag{9}$$

where θ_p is the phase angle fed to the Park transformation, θ_0 is the phase angle of the AC signal x and x_d, x_q are DC components of x on the dq-frame. In conventional droop control strategy, the phase angle θ_p is the output of droop control mode and depends on the measured active power according to (5). Due to the effect of the LPF, the angle θ_p will be different from the phase angle θ_0 of the AC quantities on the grid during transient disturbances (i.e. $\theta_0 - \theta_p \neq 0$). Therefore, x_d and x_q are not only DC signals.

Fig. 5 shows the inner current and voltage control loop including virtual output impedance in the synchronous frame. The virtual impedance can be expressed as follows.

$$\begin{cases} u_d^v = R_v \cdot i_d^g - \omega L_v \cdot i_q^g \\ u_q^v = R_v \cdot i_q^g + \omega L_v \cdot i_d^g \end{cases} \tag{10}$$

where R_v an L_v are the virtual resistance and virtual inductance, respectively, i_{dq}^g is the grid current on dq-frame. The phase angle is controlled by regulating the q-component

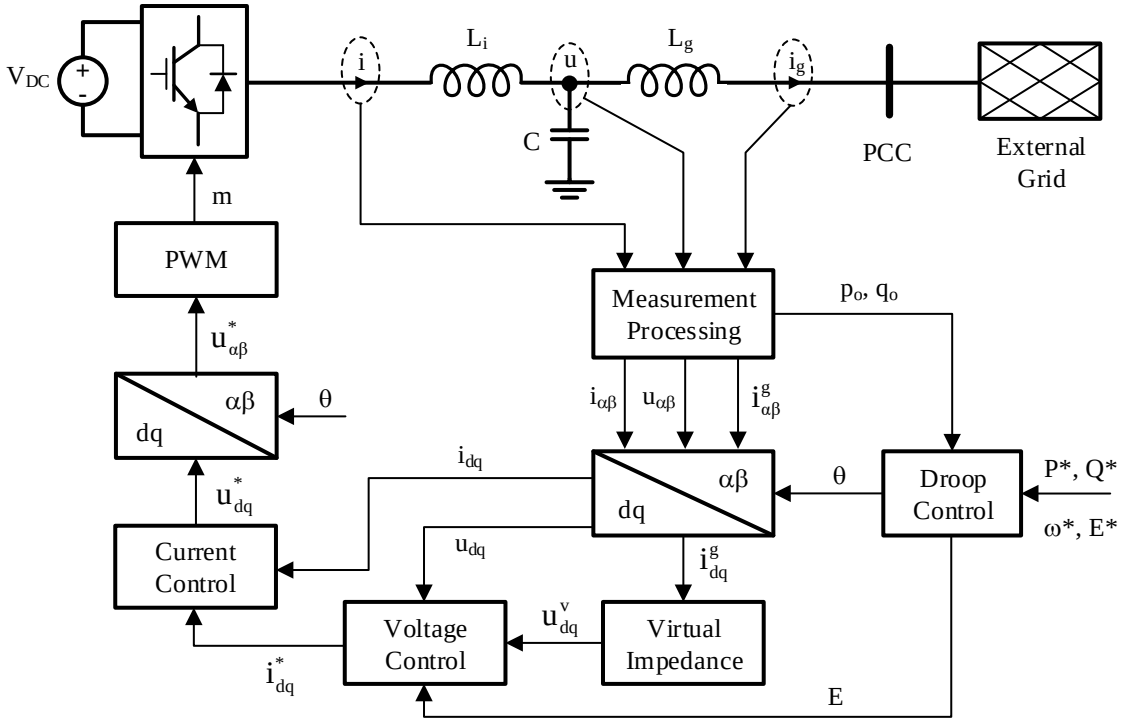

Fig. 4. Control structure of grid-forming inverters based on conventional droop control strategy

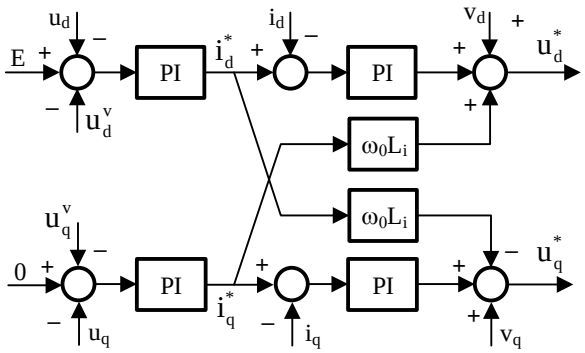

Fig. 5. Voltage and current controls with PI controller

voltage to 0, whereas the d-component voltage is controlled to trace the reference voltage magnitude.

B. *Proportional resonant (PR) controller on stationary*

PR controllers are applied directly in a stationary frame (αβ) to track sinusoidal references by providing infinite gains at the target frequencies and, therefore, ensuring almost zero steady-state error regulation. In contrast with PI controllers, PR controllers require no Park and reverse Park transformations, avoiding the transformations' errors during transient disturbances.

References [8], [9] mathematically express a process to achieve a PR controller by transforming a PI controller from a synchronous frame to a stationary frame. Therefore, the PR controller in the stationary frame should have the same performances as the PI controller in the synchronous frame. The ideal transfer function of a PR controller is expressed in (11).

$$G_{PR}(s) = k_p + k_r \frac{s}{s^2 + \omega_0^2} \tag{11}$$

where, k_p and k_r are the proportional and resonant gain constants, respectively, ω_0 is the resonant frequency (i.e. the reference frequency). The PR controller has an infinite gain at the resonant frequency so that it can achieve zero steady-state error for tracking a sinusoidal signal. Unfortunately, the ideal PR controller is challenging to be practically implemented because of the stability problem caused by infinite gain [10]. Thus, a more practical alternative is described in (12).

$$G_{PR}(s) = k_p + k_r \frac{2\omega_c s}{s^2 + 2\omega_c s + \omega_0^2} \tag{12}$$

where, ω_c is cut-off frequency. The smaller ω_c will give better harmonic extraction. However, this also leads to a higher sensitivity to frequency variations and, in consequence, slower transient response. In practice, ω_c is chosen in a range of 5–15 rad/s to achieve acceptable performance [11], being used in this paper ω_c = 5 rad/s. The purpose of using the non-ideal transfer function (12) is to theoretically limit the magnitude of gain to $|G_{PR}(j\omega_0)| = k_p + k_r$ at ω_0. The implementation of inner control loop with PR controller and virtual output impedance is shown in Fig. 6.

To adopt a completed droop control scheme with PR controller in stationary frame, the control diagram in Fig. 4 should be modified by removing the Park transformation and replacing voltage and current controls with PI controller by ones with PR controller (see Fig. 6).

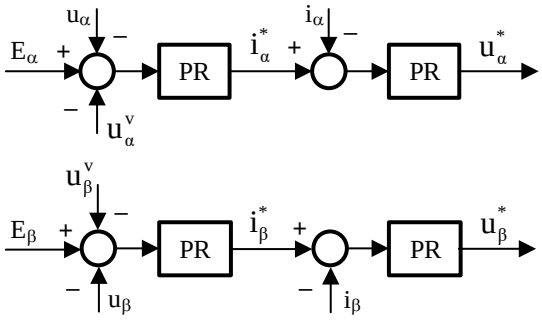

Fig. 6. Voltage and current controls with PR controller

IV. CURRENT LIMITATION METHODS

Current limitation is one of the most important criteria that must meet when considering inverters' operation. Currents in short-circuits might reach 5 to 10 times rated current [12]. As for controllers in dq-frame, several different current limitation methods are proposed and analyzed in [13], such as: "DQ component limitation" limiting d and q components of the reference current separately, "vector amplitude limitation", "switching inverters to current sources during the fault" and "virtual impedance utilization". In this paper, vector amplitude limitation is employed because of its acceptable performance and simple implementation. The basic idea of this concept is illustrated in Fig. 7, in which the output reference currents of the voltage control (as shown in Fig. 5) are reduced on both dq components simultaneously. By following the condition (13), the reference current magnitude is limited to a designed maximum current i_{max}, which is set to 2p.u. in this paper.

$$i^*_{dq\_lim} = \begin{cases} \dfrac{i_{max}}{\sqrt{i_d^{*2} + i_q^{*2}}} i^*_{dq}, if \sqrt{i_d^{*2} + i_q^{*2}} > i_{max} \\ i^*_{dq} \qquad\qquad , otherwise \end{cases} \tag{13}$$

Similarly, vector current limitation is also applied for PR controller in stationary frame by following the condition (13) in which i^*_α and i^*_β play the same roles as i^*_d and i^*_q.

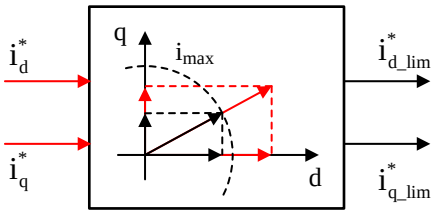

Fig. 7. Vector amplitude limitation concept

V. LCL FILTER DESIGN

An LCL-filter is applied to reduce the current harmonics caused by switching devices in the inverter. Compared to

conventional L-filters, LCL filters offer a better attenuation of harmonics at high frequencies and require smaller filter size.

LCL filters often make the control system unstable due to large magnitude peaks at resonance frequencies. Passive damping (PD) and active damping (AD) methods are generally adopted to overcome this drawback. The damping method aim to add impedances to the filters at these resonance frequencies to avoid oscillation [14]. However, the PD method causes power losses, and AD method requires more complex control strategies. For a simple damping solution, the PD method with a damping resistance R_d is mentioned in this paper. The per-phase equivalent circuit of such an LCL filter with PD method is depicted in Fig. 8. The introduced LCL filter consists of an inductor L_{inv} on the inverter side, an inductor L_g on the grid side and a filter

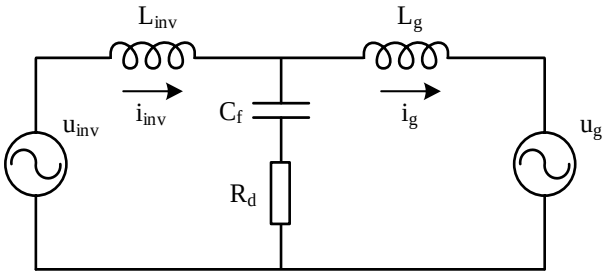

Fig. 8. Equivalent circuit of an LCL filter

capacitor C_f in series with a damping resistor R_d.

By following the LCL-filter design procedure introduced in [15], the component parameters are calculated with several rules which should be considered.

1) The maximum permissible current ripple Δi_{max} of the inverter current is limited to 10% of the nominal amplitude and the ripple value of the grid current i_g is 1% of the nominal amplitude.

2) The total inductance $(L_{inv} + L_g)$ should be less than 0.1 p.u. to make the losses and the voltage drop on the filter negligible during operation.

3) The maximum reactive power absorbed by the filter-capacitor is less than 5% of the system's rated power.

4) The resonance frequency of the filter should fulfil the condition given by (14).

$$10 \cdot f_0 < f_{res} < \frac{1}{2} \cdot f_{sw} \tag{14}$$

where, f_0 is the grid nominal frequency (in this case, 50Hz), f_{res} is the resonance frequency as given by (15) and f_{sw} is the selected switching frequency, 16kHz.

$$f_{res} = \frac{1}{2\pi} \sqrt{\frac{L_{inv} + L_g}{L_{inv} \cdot L_g \cdot C_f}} \tag{15}$$

5) To reduce the losses caused by the damping resistor, the value of damping resistor should be less than or equal to one-third of the capacitor impedance at the resonance frequency as in (16)

$$R_d \leq \frac{1}{3 \cdot 2\pi \cdot f_{res} \cdot C_f} \tag{16}$$

The calculated parameters of the filter which satisfy all of rules above are shown in TABLE I. The output of the designed LCL filter can be examined by executing the electromagnetic transients (EMT) simulation method in PowerFactory. The PWM Converter block in the software needs to switch to the Detailed Model in the EMT-Simulation tab. Besides, the minimum integration step size should be $2f_{sw}$.

Fig. 9 shows the waveforms of both inverter current and grid current whose ripples are limited to 10% and 1% of the nominal current magnitude, respectively, by using the designed LCL filter. The grid current is an approximately sinusoidal wave with negligible distortion.

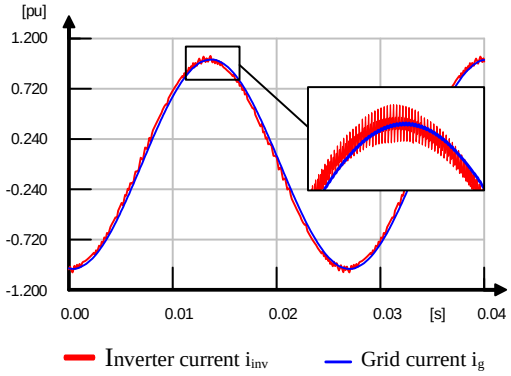

Fig. 9. Output phase current waveform of the LCL filter

VI. SIMULATION RESULTS

To validate the presented control theory in the paper, a control structure of a droop-based grid-forming inverter with other grid components is simulated in PowerFactory with the parameters of the system listed in TABLE I.

TABLE I. TESTED SYSTEM PARAMETERS

Parameters	***Value***
Rated power	40kW
Line-line voltage (RMS)	400V
DC bus voltage	800V
Grid frequency	50Hz
Switching frequency	16kHz
Inverter-side inductor	1.0mH
Grid-side inductor	0.03mH
Filter capacitor	39.8μF
Damping resistor	0.3Ω

The simulation aims to investigate the behaviors of the controller in both the synchronous frame and stationary frame under various test cases. The first four test cases are applied to the PI controller as follows:

A. Response to a step-change in active power

B. Response to a step-change in reference voltage magnitude

C. Response to a step-change in reference voltage phase angle

D. Response to a step-change in reference frequency

E. Response to a short-circuit fault

The following two test cases are conducted to evaluate the performance of the PR controller.

F. Response to a step-change in active power with droop controller in stationary frame

G. Response to a short-circuit fault with droop controller in stationary frame

The modelled power system consists of an inverter and an LCL filter connected with an AC voltage source via grid impedance. In addition, loads are connected to the point of common coupling (PCC) as shown in Fig. 10. The AC voltage source is employed as grid voltage and frequency reference. The results in each test case are presented by graphics of frequency, filter capacitor voltage, grid current, active and reactive power flowing into the PCC. Load 2 will be connected to the grid in test cases A and F, while being disconnected in other test cases. The operation point of the inverter is 50% of rated power in all test cases.

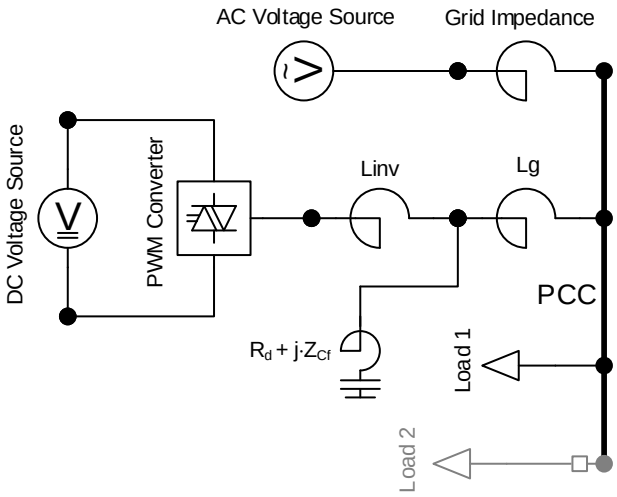

Fig. 10. Diagram of tested model in PowerFactory

A. *Response to a step-change in active power*

In this test case, load 2 will be connected at t = 0.0s, therefore the power demand will be increased from 50% to 100% of the rated power. Fig. 11 depicts the results of the test. When the transient event occurs, the loads tend to draw current from the inverter instead of the voltage source because the inverter output impedance is less than the grid impedance. Thus, the delivered active power increases, and the frequency drops due to the droop relationship. In the steady state, they are restored to the nominal values because the system frequency is maintained by the voltage source. Hence, the increasing active power will be compensated by the voltage source. However, the delivered reactive power remains deviation from the nominal value because the grid impedance consumes more reactive power due to higher current flowing through the impedance. This results in a slightly drop on the voltage magnitudes.

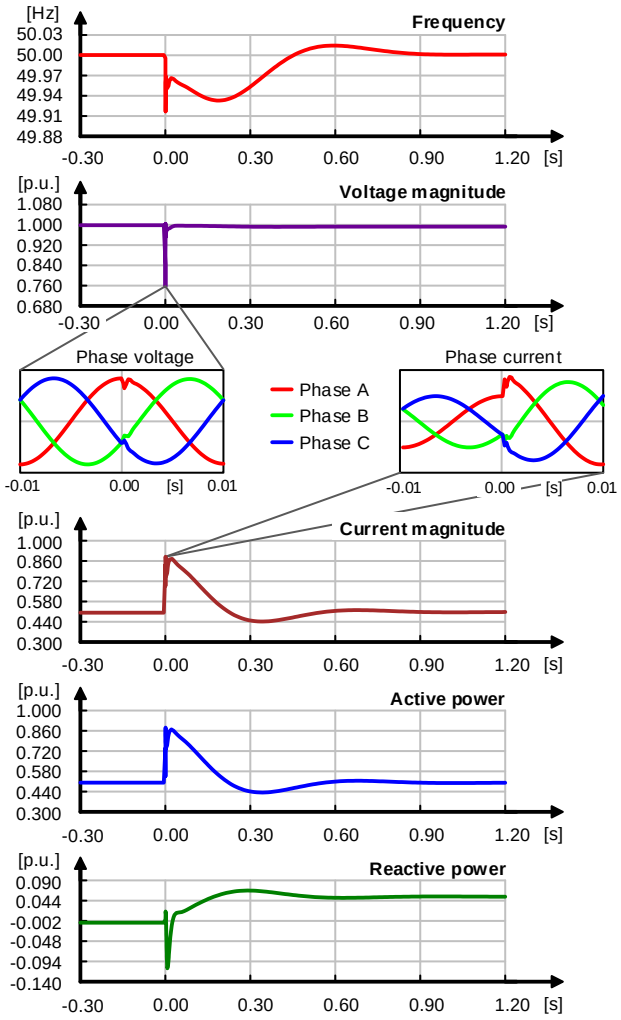

Fig. 11. Response to a step-change in active power

B. *Response to a step-change in reference voltage magnitude*

The system's reference voltage magnitude is increased by 20% at t = 0.0s, which is done by changing the voltage magnitude of the AC voltage source. The result is shown in Fig. 12. The voltage at the PCC is much lower than the reference voltage due to the voltage drop at the grid impedance. During the first few milliseconds after the transient, more current flows to the PCC from the voltage source because of the voltage difference between them. Thus, the delivered active and reactive power drop significantly. When the system reaches the steady state, the delivered active power is pulled back to the nominal value since there are no changes in the frequency. As the reference voltage magnitude increases, the reactive power magnitude is decreased to a negative value, i.e. the inverter consumes reactive power in this case. Hence, more reactive current flows through the connection line, resulting in the increase of the current magnitude after the transient.

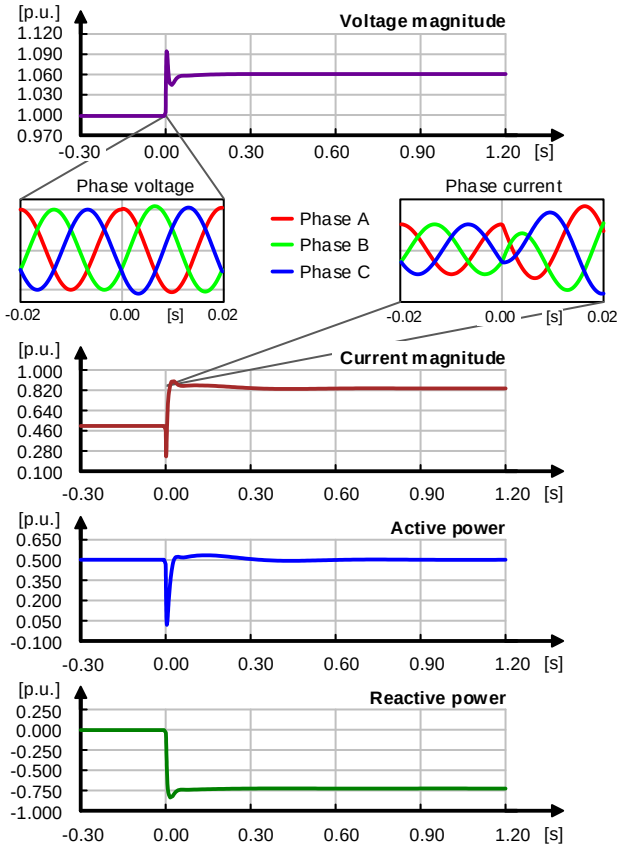

Fig. 12. Response to a step-change in reference voltage magnitude

C. *Response to a step-change in reference voltage phase angle*

The voltage phase angle of the voltage source is increased by 5^0 at t = 0.0s. Therefore, the phase angle difference δ is decreased resulting in decreasing of the delivered active power according to (1) (see Fig. 13). Thus, the inverter tries to increase the output frequency. Consequently, the phase angle of the inverter increases, resulting in boosting δ to the nominal value. Finally, the system is restored to the normal state after the transient.

D. *Response to a step-change in reference frequency*

The system's reference frequency is increased by 0.15Hz at t = 0.0s (Fig. 14). Hence the delivered active power and current magnitude are significantly decreased according to the droop relationship. That requires more current from the AC voltage source to fulfil the power demand. Hence, the voltage drop at the grid impedance increases causing the decrease of the voltage at the PCC as shown in the figure. This explains the increasing in the delivered reactive power from the inverter to the PCC.

E. *Response to a short-circuit fault*

The purpose of this test case is to verify the response of the current limitation method. Therefore, a symmetrical three phase short-circuit fault is tested, although this type of fault is less common in reality. The short-circuit event is activated at t = 0.0s and is cleared at t = 0.15s. The results are shown in Fig. 15. The observation of the current limitation shows a great ability to limit the current during the short-circuit fault.

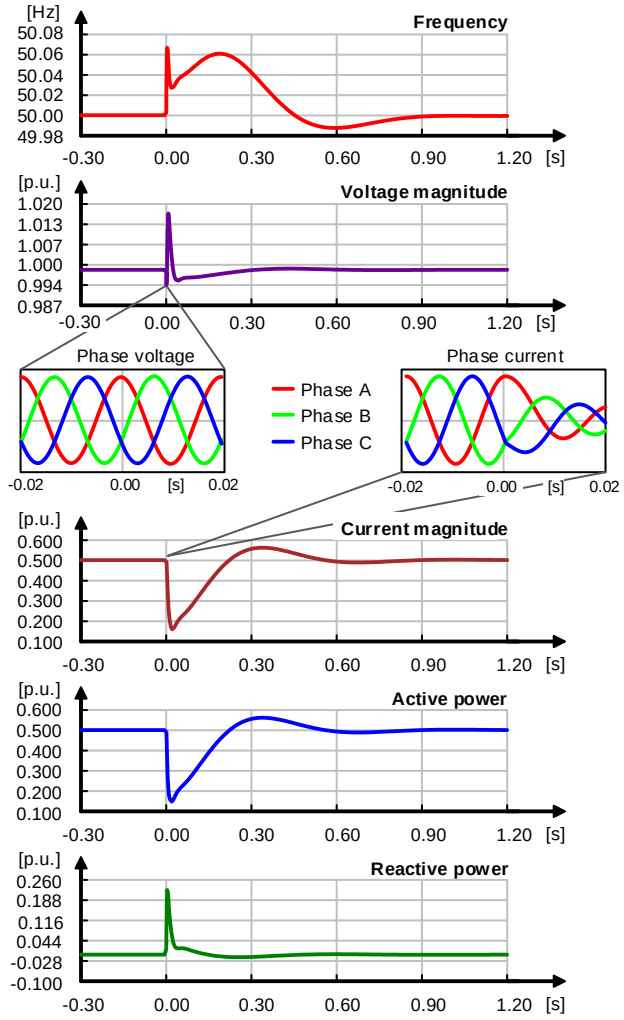

Fig. 13. Response to a step-change in reference voltage phase angle

F. *Response to a step-change in load with droop controller in stationary frame*

The result of this test case is shown in Fig. 16. It can be observed that the response of PR controller to the step-change in load is similar to the PI controller's behavior. The frequency and active power are restored to the nominal values, whereas the voltage magnitude and reactive power are shifted.

G. *Response to a short-circuit fault with droop controller in stationary frame*

Fig. 17 shows the result of the system with PR controller during a symmetrical 3 phase short-circuit fault. Although the PR controller can limit the current for most of the time, a ripple appears during the first a few milliseconds after the transient. Since the ripple reaches to current peak of 4 p.u., this transient behavior may be dangerous, especially in case of a very sensitive system. Thus, a better current limitation method for PR controller should be adopted in future work

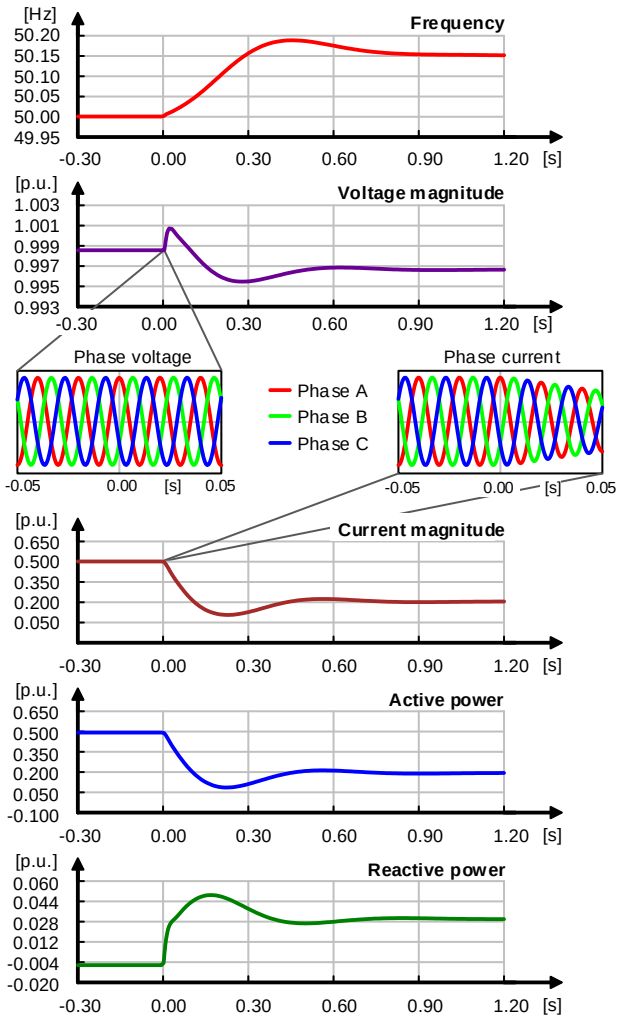

Fig. 14. Response to a step-change in reference frequency

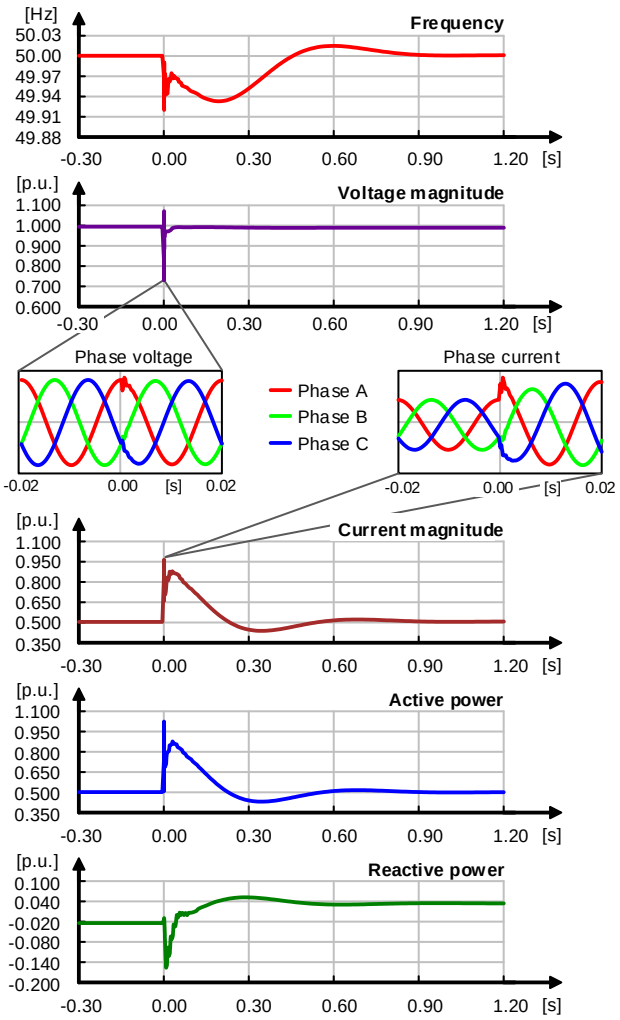

Fig. 16. Response to a step-change in active power with PR controller

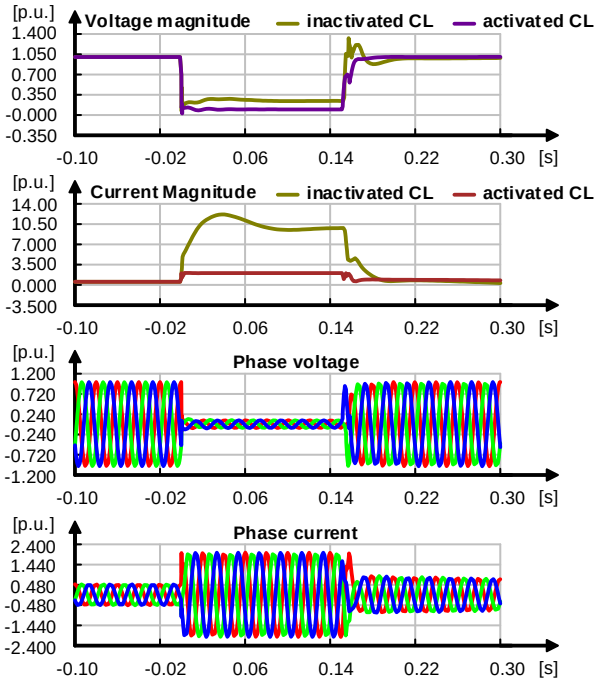

Fig. 15. Response to a short-circuit fault

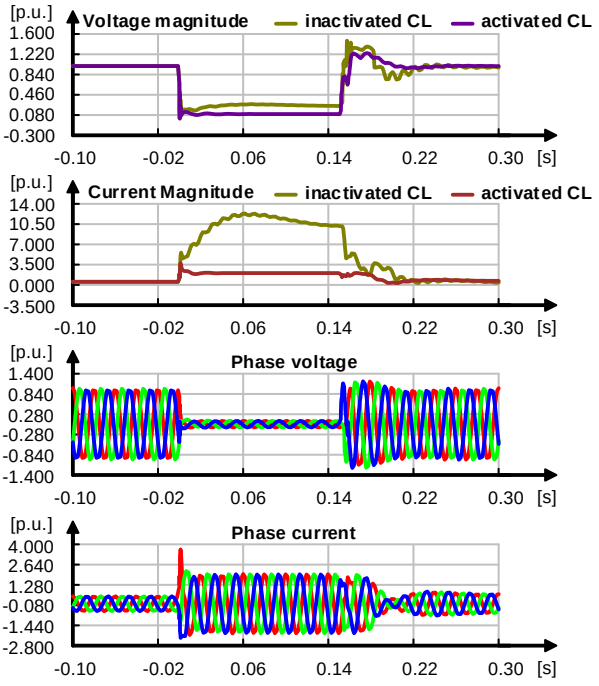

Fig. 17. Response to a short-circuit fault with PR controller

VII. CONCLUSION

In this paper, droop control schemes have been reviewed and evaluated throughout various test cases in PowerFactory. The controllers enable synchronization to an existing network or other voltage sources as well as load sharing between different generators in islanded mode. At the lowest control level, voltage regulation is implemented, which has a special current limiting function to limit the output current in the event of errors such as short circuits or overload situations. With droop control, grid-forming inverters are proved to be able to replace the properties of the discontinued synchronous generators.

Simulation shows that PI controllers on synchronous frame and PR controllers on stationary frame have similar performances under fundamental changes of the grid. The PR technique requires no transformations and less computation, that makes the controller schemes more simple and easier for implementation. However, the current method applied for the PR controller has limitation of eliminating ripples on the current magnitude. Therefore, a better method for the PR controller should be studied in future work. Whereas, the presented current limitation method based on the vector amplitude limitation shows an excellent performance for PI controller in synchronous frame.

ACKNOWLEDGMENT

The presented work was financially supported by the German Federal Ministry for Economic Affairs and Energy under the project number 0350015A (VerbundnetzStabil).

REFERENCES

[1] Tayyebi, Ali & Dörfler, Florian & Kupzog, Friederich & Miletic, Zoran & Hribernik, Wolfgang, “Grid-Forming Converters -- Inevitability, Control Strategies and Challenges in Future Grid Applications”, 2018.

[2] J. M. Guerrero, L. Hang and J. Uceda, "Control of Distributed Uninterruptible Power Supply Systems," in IEEE Transactions on Industrial Electronics, vol. 55, no. 8, pp. 2845-2859, Aug. 2008.

[3] J. Rocabert, A. Luna, F. Blaabjerg and P. Rodríguez, "Control of Power Converters in AC Microgrids," in IEEE Transactions on Power Electronics, vol. 27, no. 11, pp. 4734-4749, Nov. 2012.

[4] F. K. A. Lima, C. G. C. Branco, J. M. Guerrero, L. J. C. B. C. Neto, S. S. Carvalho and R. P. Torrico-Bascopé, "Analysis, modelling, and simulation of droop control with virtual impedance loop applied to parallel UPS systems," IECON 2013 - 39th Annual Conference of the IEEE Industrial Electronics Society, Vienna, pp. 1524-1529, 2013.

[5] Brabandere, K. De et al. “A Voltage and Frequency Droop Control Method for Parallel Inverters.” IEEE Transactions on Power Electronics 22: 1107-1115, 2007.

[6] S. D'Arco and J. A. Suul, "Virtual synchronous machines — Classification of implementations and analysis of equivalence to droop controllers for microgrids," 2013 IEEE Grenoble Conference, Grenoble, pp. 1-7, 2013.

[7] J.G., Dragičević, T., Meng, L., Blaabjerg, F. and Li, Y., “Control of Power Converters in ac and dc Microgrids”, Wiley Encyclopedia of Electrical and Electronics Engineering, J.G. Webster (Ed.), 2020.

[8] Burger, Bruno & Engler, Alfred, “Fast signal conditioning in single phase systems”, 2001.

[9] D. N. Zmood and D. G. Holmes, "Stationary frame current regulation of PWM inverters with zero steady-state error," in IEEE Transactions on Power Electronics, vol. 18, no. 3, pp. 814-822, May 2003.

[10] Vu, Trung-Kien & Seong, Se-Jin., “PR Controller Based Current Control Scheme for Single-Phase Inter-Connected PV Inverter”. Journal of the Korea Academia-Industrial cooperation Society, 2009.

[11] P. C. Tan, P. C. Loh and D. G. Holmes, "High-Performance Harmonic Extraction Algorithm for a 25 kV Traction Power Quality Conditioner," in IEE Proceedings - Electric Power Applications, vol. 151, no. 5, pp. 505-512, 9 Sept. 2004.

[12] Duckwitz, Daniel & Welck, Friedrich & Glöckler, Christoph & Knobloch, Andreas & Becker, Tobias & Bülo, Thorsten, “Experimental Short-Circuit Testing of Grid-Forming Inverters in Microgrid and Interconnected Mode”, 2018.

[13] A. Gkountaras, S. Dieckerhoff and T. Sezi, "Evaluation of current limiting methods for grid forming inverters in medium voltage microgrids," 2015 IEEE Energy Conversion Congress and Exposition (ECCE), Montreal, QC, pp. 1223-1230, 2015.

[14] M. Liserre, F. Blaabjerg and S. Hansen, "Design and control of an LCL-filter-based three-phase active rectifier," in IEEE Transactions on Industry Applications, vol. 41, no. 5, pp. 1281-1291, Sept.-Oct. 2005.

[15] A. Reznik, M. G. Simões, A. Al-Durra and S. M. Muyeen, "LCL Filter Design and Performance Analysis for Grid-Interconnected Systems," in IEEE Transactions on Industry Applications, vol. 50, no. 2, pp. 1225-1232, March-April 2014.